Huntington disease skeletal muscle is hyperexcitable owing to chloride and potassium channel dysfunction

Christopher W. Waters, Grigor Varuzhanyan, Robert J. Talmadge, and Andrew A. Voss[1]

Department of Biological Sciences, California State Polytechnic University, Pomona, CA 91768

Edited by Kurt G. Beam, University of Colorado at Denver, Aurora, CO, and approved April 19, 2013 (received for review November 17, 2012)

Huntington disease is a progressive and fatal genetic disorder with debilitating motor and cognitive defects. Chorea, rigidity, dystonia, and muscle weakness are characteristic motor defects of the disease that are commonly attributed to central neurodegeneration. However, no previous study has examined the membrane properties that control contraction in Huntington disease muscle. We show primary defects in ex vivo adult skeletal muscle from the R6/2 transgenic mouse model of Huntington disease. Action potentials in diseased fibers are more easily triggered and prolonged than in fibers from WT littermates. Furthermore, some action potentials in the diseased fibers self-trigger. These defects occur because of decreases in the resting chloride and potassium conductances. Consistent with this, the expression of the muscle chloride channel, ClC-1, in Huntington disease muscle was compromised by improper splicing and a corresponding reduction in total *Clcn1* (gene for ClC-1) mRNA. Additionally, the total *Kcnj2* (gene for the Kir2.1 potassium channel) mRNA was reduced in disease muscle. The resulting muscle hyperexcitability causes involuntary and prolonged contractions that may contribute to the chorea, rigidity, and dystonia that characterize Huntington disease.

trinucleotide repeat | myotonia | myopathy | channelopathy | electrophysiology

Huntington disease (HD) is a debilitating and progressive disorder that develops in most patients during middle age; the more extreme form of the disease develops in juveniles (1, 2). There is currently no cure for the disease, which is characterized by severe motor and cognitive defects. The motor symptoms include chorea (irregular jerky movements), rigidity or rigor, and dystonia (abnormal tonicity often resulting in abnormal positioning of the head and limbs). These defects are the result of involuntary and prolonged contractions. Examinations of HD skeletal muscle have demonstrated atrophy, metabolic and mitochondrial defects, nonspecific histological abnormalities, and a loss of strength (3–12). Far more studies of HD have focused on the central nervous system, and the motor defects are widely considered to be the result of neurodegeneration (1, 2, 8). However, no previous study has examined the basic membrane properties in HD muscle that control action potential initiation and propagation. A normal skeletal muscle contraction requires that action potentials initiated at the neuromuscular junction propagate along the surface membrane and into the interior of the muscle fiber through the transverse tubular system. The responsiveness of the muscle to neuronal stimulation and the shape of each action potential repolarization are determined by potassium and chloride conductances, which set and maintain the resting membrane potential of skeletal muscle (13). In effect, the inward rectifying potassium (Kir) and chloride conductances buffer the membrane potential at rest. If they are reduced, the membrane becomes hyperexcitable, and normally subthreshold events can initiate action potentials and involuntary contractions. Most of the resting conductance in skeletal muscle is mediated by chloride through the muscle chloride channel (ClC-1), and a large decrease in this conductance results in the hyperexcitability, involuntary contractions, rigidity, and persistent contractions that characterize general myotonia at the cellular level (14–20).

We examined action potentials, as well as ClC-1 and Kir conductances, in dissociated ex vivo adult skeletal muscle fibers from transgenic HD mice and from age-matched WT littermates. The HD muscle came from the R6/2 transgenic mouse line, which carries the human HD gene (21) and exhibits many of the motor and cognitive defects found in HD patients (2, 22). In humans, HD is caused by an expanded CAG trinucleotide repeat in the huntingtin gene (*IT15*) (22). Patients with >40 CAG repeats develop the disease during middle age; those with >50 CAG repeats develop a more extreme juvenile form of the disease (1, 2). Because of the rapid onset of reduced activity at 4.5 wk of age (22, 23) and overt motor defects at 8 wk of age (24–26), the R6/2 line most closely models the juvenile form of HD. The R6/2 line is often considered the model of choice for preclinical trials of potential HD therapeutics owing to its rapidly developing and well-described phenotype (1). Last, because an expanded trinucleotide repeat has been shown to disrupt *Clcn1* (gene for ClC-1) mRNA processing in myotonic dystrophy type 1 (27–36), we determined whether there was a disruption in *Clcn1* mRNA processing in HD muscle. We reveal defects in HD muscle that cause hyperexcitability and may contribute to the severe involuntary and prolonged contractions that are hallmarks of the disease.

Results

We performed all electrophysiological experiments on individual dissociated HD and WT *flexor digitorum brevis* or *interosseous* muscle fibers using two intracellular microelectrodes (Fig. S1). The HD mice averaged 12 wk of age, and the WT mice averaged 13 wk of age.

Action Potentials. An action potential is the basis of excitability and the physiological signal that initiates muscle contraction. We measured action potentials in HD (n = 12) and WT fibers (n = 17) by injecting a series of depolarizing current pulses through a current-passing electrode and measuring the membrane potential with a voltage-sensing electrode (Fig. 1). This simulates the physiological condition whereby an inward current through acetylcholine receptors at the neuromuscular junction triggers an action potential. Our series of 0.5-ms current pulses ranged in amplitude from subthreshold to suprathreshold. There was a striking prolongation of the repolarization phase in HD compared with WT fibers (Fig. 1*A*). The slower time constant of the repolarization to the resting membrane potential of HD fibers (15.0 ± 2.1 ms) was nearly double that of WT (7.7 ± 0.4 ms) (Fig. 1*B* and Table 1). The HD fibers were also hyperexcitable compared with WT: the minimum current pulse required to trigger an action potential was significantly less in HD than in WT fibers

Author contributions: R.J.T. and A.A.V. designed research; C.W.W., G.V., R.J.T., and A.A.V. performed research; C.W.W., G.V., R.J.T., and A.A.V. analyzed data; and A.A.V. wrote the paper.

The authors declare no conflict of interest.

This article is a PNAS Direct Submission.

[1]To whom correspondence should be addressed. E-mail: aavoss@csupomona.edu.

This article contains supporting information online at www.pnas.org/lookup/suppl/doi:10.1073/pnas.1220068110/-/DCSupplemental.

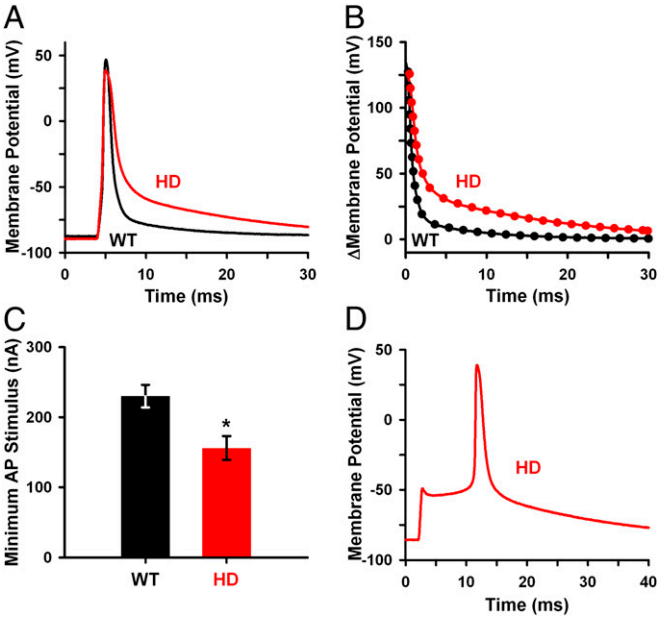

Fig. 1. Action potentials from WT and HD fibers. (*A*) Representative WT and HD action potentials showing the rising and falling phases. (*B*) Repolarization phase of the action potentials from *A* plotted with the WT (black dotted line) and HD (red dotted line) curve fits. (*C*) Minimum 0.5-ms depolarizing stimulus current (mean ± SEM) needed to trigger an action potential (AP) in WT ($n = 17$) and HD ($n = 12$) fibers. (*D*) Representative spontaneous action potential that self-triggered after an apparent subthreshold stimulus. *Significant difference compared with WT fibers ($P < 0.05$).

(Fig. 1*C*). We also observed an after-depolarization in four of the HD fibers following an apparent subthreshold current pulse, which resulted in a spontaneous action potential (Fig. 1*D*). The spontaneous action potentials occurred at an average of 6.4 ± 1.7 ms after the termination of the stimulating current pulse. In all of the action potentials, there were no significant differences in the maximum rate-of-rise or peak amplitude, suggesting that the effects we measured were not due to changes in the function and/or density of the fast voltage-gated sodium channels in HD fibers (Table 1).

The prolonged repolarization, hyperexcitability, and spontaneous action potentials would be expected if there was a reduction in the resting muscle chloride conductance through ClC-1 ($G_{ClC\text{-}1}$). The presence of self-triggered action potentials after only subthreshold stimuli indicates a pronounced hyperexcitability in HD muscle. This could occur if there was also a reduction in the inward rectifying potassium conductance (G_{Kir}). The slight but significant increase in the initial repolarization time constant of the HD action potentials could also be the result of decreases in $G_{ClC\text{-}1}$ and G_{Kir} (Table 1).

Chloride Channels. We measured chloride currents (I_{Cl}) from 9 HD and 14 WT fibers using a three-pulse voltage clamp protocol (Fig. 2*A*) that accounted for the voltage- and time-dependent deactivation of ClC-1 (37–40). To ensure large inward currents, we used high intracellular chloride (70 mM). From a holding potential of −20 mV, the chloride equilibrium potential, we applied a depolarizing conditioning pulse (P1) that was followed by two consecutive test pulses (P2 and P3). P1 fully activated the chloride channels. We then used P2 to determine the voltage dependence of the instantaneous or peak currents through the open channels. After the channels deactivated, we used the currents at the onset of P3 to determine the relative open probability of the chloride channels. The resulting average specific currents (μA/cm^2) are shown in Fig. 2 *B–D*. To isolate the chloride currents, we blocked the major Na^+, K^+, and Ca^{2+} channels with tetrodotoxin, Cs^+ substitution, and nifedipine, respectively. The specific I_{Cl} (Fig. 2*D*) was the difference between the currents recorded before (Fig. 2*B*) and during (Fig. 2*C*) exposure to the chloride channel blocker anthracene-9-carboxylic acid (9AC).

There was a clear reduction in the specific I_{Cl} and $G_{ClC\text{-}1}$ of HD compared with WT fibers (Fig. 2*D*). The peak I_{Cl} at −140 mV during P2 in HD fibers (−360 ± 48 μA/cm^2) was significantly smaller than the mean value in WT (−1,133 ± 72 μA/cm^2) ($P < 0.001$). To determine $G_{ClC\text{-}1}$ we examined the current–voltage (IV) relationship of the peak I_{Cl} values during P2 (Fig. 2*E*). The peak $G_{ClC\text{-}1}$, the slope of the IV relationship from −100 to −140 mV, was significantly reduced in HD fibers (4.0 ± 0.5 mS/cm^2) compared with WT (11.9 ± 0.8 mS/cm^2) ($P < 0.001$).

We also examined the average ClC-1 steady-state values, deactivation kinetics and the corresponding outward Cl^- movement, and the peak I_{Cl} kinetics (Fig. S2). Generally the results indicate that any change in ClC-1 function in HD fibers was minor compared with the marked reduction total ClC-1 currents. This was also demonstrated by the chloride channel relative open probability, which we determined by plotting the peak currents at the onset of P3 (normalized to the maximum current) as a function of the steady-state voltages from P2 (Fig. 2*F*). The relative open probability data were fitted with a Boltzmann curve. The resulting mean $V_{0.5}$ values for the HD (−41 ± 4 mV) and WT (−41 ± 3 mV) fibers were not significantly different ($P = 0.88$). The small difference in slope factors (k values) for HD (27 ± 1 mV) and WT (24 ± 1 mV) fibers ($P = 0.02$) suggests a minor change in ClC-1 function in HD fibers.

Inward Rectifying Potassium Channels. We measured the specific Kir currents (I_{Kir}) from HD ($n = 11$) and WT ($n = 12$) fibers (Fig. 3). Kir channels are unique because their opening depends on the membrane potential and the extracellular [K^+] (41). At potentials negative to the potassium equilibrium potential (E_K), the Kir channels open and generate inward currents; whereas, at potentials positive to E_K, the channels are mostly closed. To generate large inward currents, we used high extracellular K^+ (130 mM). The E_K was −9.5 mV. We measured I_{Kir} from a holding potential of 0 mV by applying large negative and small positive pulses (Fig. 3*A*). To isolate the potassium currents, we blocked the major Na^+, Cl^-, and Ca^{2+} channels with tetrodotoxin, 9AC, and nifedipine, respectively. The specific I_{Kir} (Fig. 3*B*)

Table 1. Action potential properties of HD and WT fibers

Parameter	Resting membrane potential (mV)	Max rate-of-rise (mV/ms)	Max Δvoltage (mV)	Decay τ_1 (ms)	Decay τ_2 (ms)
WT ($n = 17$)	−87 ± 1	420 ± 33	127 ± 3	0.62 ± 0.04	7.7 ± 0.4
HD ($n = 12$)	−86 ± 1	465 ± 47	125 ± 2	0.82 ± 0.06*	15.0 ± 2.1*

Average values (±SEM) of the resting or baseline membrane potential, the maximum rate-of-rise of the depolarization, the peak change in membrane potential, the initial repolarization time constant (τ_1), and the slower repolarization time constant (τ_2). * indicates a significant difference compared to WT fibers ($P < 0.05$).

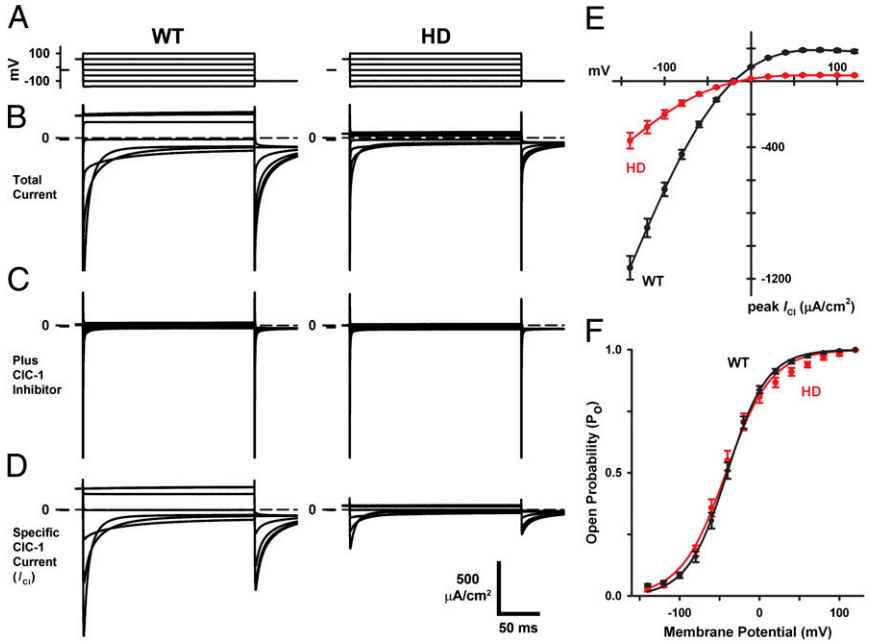

Fig. 2. Average chloride currents of WT ($n = 14$) and HD ($n = 9$) fibers. (*A–D*) Voltage clamp traces for WT (*Left*) and HD (*Right*) fibers. (*A*) Voltage protocol with a holding potential of −20 mV, a break during the 150-ms conditioning pulse to +60 mV (P1), a second 200-ms test pulse with steps from −140 to +120 mV in +20-mV increments (P2), and a third 50-ms test pulse to −100 mV (P3). For clarity, only half the traces are shown in *A–D*. (*B–D*) Current records normalized to fiber surface area (cm^2). (*B*) Total currents composed of the chloride current (I_{Cl}) plus leak and capacitive currents. (*C*) Leak and capacitive currents measured by blocking chloride channels with 400 μM 9AC. For scaling purposes, the full capacitive transients in *B* and *C* are not shown. (*D*) Specific I_{Cl} records obtained by subtracting the leak and capacitive currents (*C*) from the total currents (*B*). (*E*) IV relationship of the peak I_{Cl} (mean ± SEM) from P2 for WT and HD fibers. $G_{ClC\text{-}1}$ was the slope of the IV relationship from −100 to −140 mV. (*F*) Relative open probability of WT and HD chloride channels (mean ± SEM) obtained by plotting the normalized peak currents from P3 as a function of steady-state voltage from P2. The WT and HD data were each fitted with a Boltzmann curve.

was the difference between the currents recorded before and during exposure to the Kir channel blocker, Ba^{2+} (Fig. S3).

The IV relationship of the peak I_{Kir} values is shown in Fig. 3*C*. The peak I_{Kir} at −60 mV in HD (−87 ± 11 μA/cm^2) was significantly less than in WT fibers (−216 ± 12 μA/cm^2) ($P < 0.001$). The peak G_{Kir}, the slope of the peak I_{Kir} values from −40 to −60 mV, was significantly less in HD (1.8 ± 0.2 mS/cm^2) than in WT fibers (4.3 ± 0.2 mS/cm^2) ($P < 0.001$). The decline in I_{Kir} at large negative voltage pulses (Fig. 3*B*) was likely the result of K^+ depletion in the transverse tubular system (42). A decrease of G_{Kir} should slow the rate at which the I_{Kir} declines. Accordingly, I_{Kir} declines at a slower rate in HD than WT fibers (Fig. S3*E*). Our results are consistent with a previous study showing a reduced Kir current density in striatal medium-sized spiny neurons in R6/2 HD mice (43).

To more fully assess the decreases in $G_{ClC\text{-}1}$ and G_{Kir} as well as the membrane properties, we analyzed the capacitance. The amount of plasma membrane is generally considered to be directly proportional to the capacitance of the fiber. Thus, current

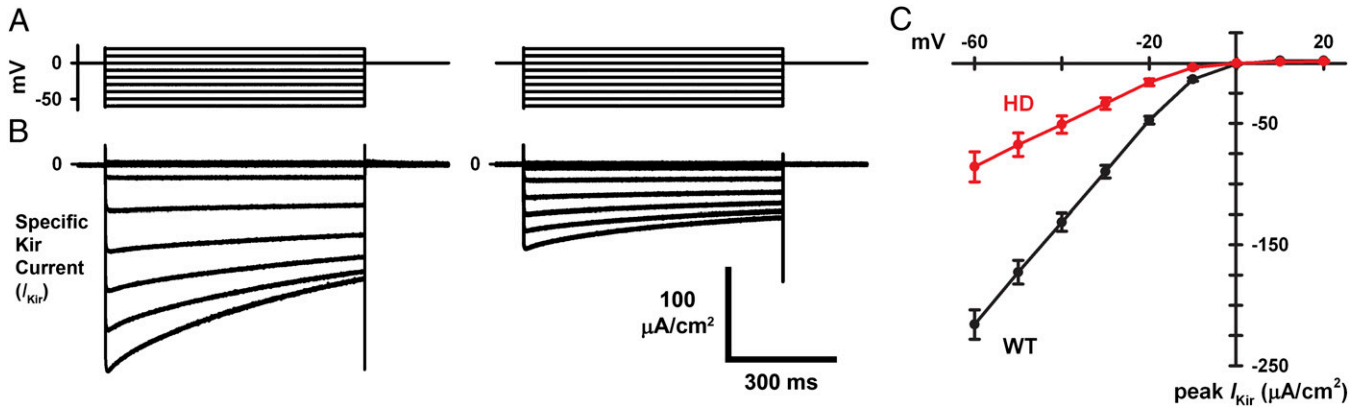

Fig. 3. Average inward rectifying potassium currents of WT ($n = 12$) and HD ($n = 11$) fibers. (*A* and *B*) Voltage clamp traces for WT (*Left*) and HD (*Right*) fibers. (*A*) Voltage protocol with a holding potential of 0 mV and a series of 700-ms steps from −60 to +20 mV in +10-mV increments. (*B*) Specific inward rectifying potassium (I_{Kir}) currents obtained by recording the total currents and subtracting the leak and capacitive currents (analogous to method for obtaining I_{Cl}). Leak and capacitive currents records were made by blocking inward rectifying potassium channels with 5 mM Ba^{2+}. (*C*) IV relationship of the peak I_{Kir} (mean ± SEM) from *B* for WT and HD fibers. G_{Kir} was the slope of the IV relationship from −40 to −60 mV.

levels are often normalized to total fiber capacitance and reported as current densities.

Specific Capacitance and Current Densities. We measured capacitance by integrating capacitive transients in the same fibers used to study $G_{ClC\text{-}1}$ and G_{Kir} under conditions whereby the chloride and potassium channels were blocked (Fig. S4). This minimized the errors due to voltage-activated channels. The capacitance of HD and WT fibers were compared by normalizing to total fiber surface area to obtain the specific capacitance (C_m). The specific chloride and K_{ir} currents listed above were obtained the same way. For each fiber, we estimated the surface area using an image that included the fiber length and diameter (Fig. S1) and assuming the fiber was cylindrical. If the surface membrane accounted for all of the plasma membrane, the C_m of muscle would be ~1 μF/cm^2. In muscle, the C_m is higher because of the transverse tubular system, a series of invaginations of the surface membrane that spread radially into the interior of the fiber.

C_m was significantly lower in HD (3.4 ± 0.2 μF/cm^2, n = 20) than in WT fibers (5.1 ± 0.2 μF/cm^2, n = 26) ($P < 0.001$). A smaller average diameter of the HD fibers may contribute to, but does not likely explain, the full decrease in C_m (Table S1). The decreased C_m of HD fibers suggests there was a reduction of the transverse tubular system (detubulation) in the diseased muscle. Because detubulation could cause decreases in membrane conductance, we also normalized the ClC-1 and Kir results to total fiber capacitance. The HD $G_{ClC\text{-}1}$ (1.0 ± 0.1 mS/μF) and G_{Kir} (0.6 ± 0.1 mS/μF) values normalized to capacitance were significantly less than the WT $G_{ClC\text{-}1}$ (2.4 ± 0.2 mS/μF, $P < 0.001$) and G_{Kir} (0.9 ± 0.1 mS/μF, $P = 0.008$). The decreases in $G_{ClC\text{-}1}$ and G_{Kir} (when normalized to capacitance) should be independent of fiber diameter. Thus, the density of functional ClC-1 and Kir channels in HD fibers was reduced.

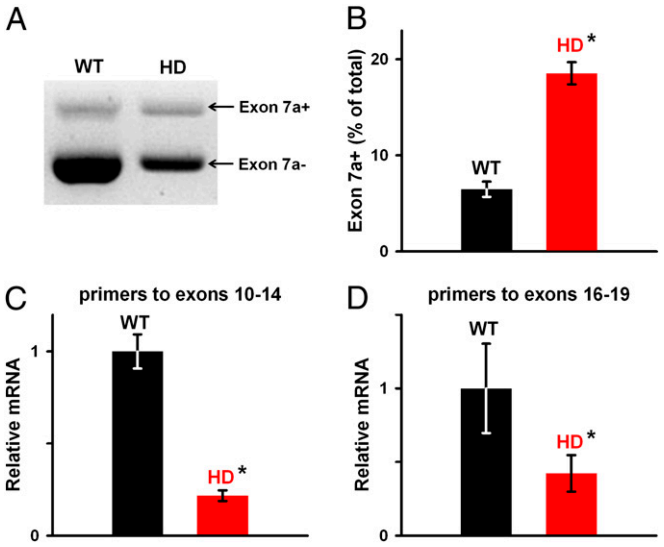

Fig. 4. Reduced expression of *Clcn1* mRNA in HD muscle coincides with atypical splicing of *Clcn1* pre-mRNA. (*A*) Gel showing aberrantly spliced *Clcn1* mRNA that contains exon 7a (Exon 7a+, 420 bp) and normal adult *Clcn1* mRNA that lacks exon 7a (Exon 7a–, 341 bp) in WT (*Left*) and HD *interosseous* (*Right*) muscle. (*B*) Aberrant *Clcn1* mRNA with exon 7a was expressed at higher proportional levels in the HD (n = 2) compared with WT (n = 3) muscle. (*C* and *D*) The relative expression of total *Clcn1* mRNA, normalized to β2-microglobulin using the ΔΔCT method, was significantly reduced in HD muscle as determined by real-time RT-PCR using two separate primer sets spanning exons 10–14 or exons 16–19. *Significant difference compared with WT muscle ($P < 0.05$). Average values (± SEM) of the resting or baseline membrane potential, the maximum rate-of-rise of the depolarization, the peak change in membrane potential, the initial repolarization time constant (τ_1), and the slower repolarization time constant (τ_2). *Significant difference compared with WT fibers ($P < 0.05$).

mRNA Analysis. The loss of chloride channels in myotonic dystrophy is thought to be due to an accumulation of RNA with CUG or CCUG repeats in the nucleus that disrupt the function of RNA binding proteins, such as muscleblind-like 1 and 2; consequently, aberrantly spliced *Clcn1* mRNA that contains exon 7a is degraded via nonsense-mediated decay (27–36). We tested for this mechanism in HD *interosseous* muscle (Fig. 4). We found a nearly threefold increase in the proportion of aberrantly spliced *Clcn1* mRNA (containing exon 7a) in HD compared with WT muscle (Fig. 4 *A* and *B*). A similar increase was found in *extensor digitorum longus* muscle (Fig. S5). Additionally, the total level of normal *Clcn1* mature mRNA, determined using two separate primer sets, was significantly reduced in HD compared with WT muscle (Fig. 4 *C* and *D*). Similarly, the level of mRNA for the gene that encodes the Kir 2.1 potassium channel (*Kcnj2*) was significantly reduced in the HD *interosseous* muscle (0.186 ± 0.005) (n = 2) relative to WT (1.000 ± 0.181) (n = 3) ($P = 0.04$) and in the HD *extensor digitorum longus* muscle (0.495 ± 0.074) (n = 2) relative to WT (1.000 ± 0.071) (n = 3) ($P = 0.02$).

Discussion

We examined the fundamental membrane properties that govern the responsiveness of HD muscle to neuronal stimulation and initiate contraction. There were significant decreases in $G_{ClC\text{-}1}$ and G_{Kir}, which account for most of the resting conductance in muscle and keep the membrane potential near resting levels (13). For example, triggering an action potential requires that excitatory currents overcome $G_{ClC\text{-}1}$ and G_{Kir}. Thus, the reductions in $G_{ClC\text{-}1}$ and G_{Kir} explain the reduced current required to trigger an action potential in HD fibers. The decreased conductances also explain the prolonged falling phase of the action potentials in HD fibers: currents through chloride and Kir channels help drive the membrane potential back to resting levels during the repolarization phase. For the same reasons, the decreases in $G_{ClC\text{-}1}$ and G_{Kir} explain the increased input resistance and membrane time constant previously reported for *flexor digitorum brevis* fibers from R6/2 mice (6). We confirmed those results using a similar procedure (Table S2).

A previous study found reductions in muscle ClC-1 (likely mediated by myogenic factors) that occurred 2 d after denervation (17). Could the defects we report be related to denervation or motor neuron degeneration? This seems very unlikely because a previous study, using the same muscle tissue, demonstrated that neuromuscular innervation was normal throughout the life of the R6/2 mice, which occurred despite significant, uniform, and progressive muscle atrophy (6). Moreover, the same study found that the R6/2 mice maintained a normal ability to regenerate motor axons and functional neuromuscular junctions after crushing the tibial nerve. The normal innervation of HD muscle indicates that the defects reported in this study were independent of denervation and motor neuron degeneration.

We found greater percent decreases in $G_{ClC\text{-}1}$ and G_{Kir} when normalized to surface area rather than to capacitance. This could occur if some of the ClC-1 and Kir channels were lost simply because of a decrease in the transverse tubular system. Indeed, a partial detubulation in the HD fibers was suggested by the decrease in C_m and the faster time-to-peak of the ClC-1 and Kir channel currents (Figs. S2*E* and S3*F* and Table S1). Whereas there are conflicting reports about the location of ClC-1 in muscle (37, 40), it is established that Kir channels are expressed in the transverse tubular system (44, 45). A definitive confirmation of a partial detubulation will require optical methods that include electron microscopy.

In summary, a key finding of this study is that the decreased resting conductances cause hyperexcitability in HD muscle. The degree of hyperexcitability was high enough to cause self-triggering action potentials that occurred after apparent subthreshold stimuli. We found minimal disruption of ClC-1 and Kir function in HD fibers (Figs. S2 and S3), suggesting that the decreased conductances were caused by a reduced expression of ClC-1 and Kir channels. Consistent with this, we found reduced levels of normal mature *Clcn1* and *Kcnj2* mRNA. A disruption of mRNA splicing has been shown to cause a decrease in ClC-1 expression in myotonic dystrophy type 1, another trinucleotide repeat disorder (27–36). We measured elevated levels of aberrant *Clcn1* mRNA containing exon 7a in HD muscle, which indicates a similar disruption in *Clcn1* pre-mRNA splicing. At the cellular level, we have found striking biophysical and molecular similarities between HD and myotonic dystrophy muscle, suggesting, to some degree, that there is a common pathophysiology that involves a disruption in RNA processing. It will be interesting in future studies to determine the factors that result in similar but distinct clinical phenotypes in the diseases. The hyperexcitability and decreased conductances that we identified reveal a primary myopathy that may contribute to the motor defects of HD.

Materials and Methods

Animal Care and Use. All animal procedures were performed in accordance with the policies of the Animal Care and Use Committee of the California State Polytechnic University, Pomona. Five-week-old female R6/2 [B6CBA-Tg (HDexon1)62Gpb/1J hemizygous] and WT sibling mice were ordered from The Jackson Laboratory and cared for according to published reports (6, 21). We used a total of 14 HD mice that ranged in age from 78 to 88 d (average age of 12 wk) and 15 WT mice that ranged in age from 73 to 100 d (average age of 13 wk). The date of birth information from The Jackson Laboratory was ±3 d.

Upon arrival animals were housed with like-genotype littermates in cages supplied with filtered air within an isolation rack (Innovive). The cages contained irradiated ¼-inch corn cob bedding (Harlan Teklad 7902) and environmental enrichment (mouse house and cotton nestlet). Mice were supplied with dry chow (Irradiated Rodent Diet; Harlan Teklad 2918) and water ad libitum. At 10 wk of age, the HD mice were supplied with supplemental food and water in the form of Hydrogel and mash (dry chow moistened until paste-like in consistency) placed on the cage floor. Environmental conditions were maintained with a 12-h day/night cycle and constant temperature (21–23 °C) and humidity (55% ± 10%). Cages were changed every 2 wk or as needed.

The behavior and physical condition of the mice were tested weekly until 10 wk of age and then daily until the animals were selected for experiments. Testing categories were physical condition, approximate respiratory rate and effort, activity level, consumption of water and food, weight loss, and hind limb clasping. Each category was rated on a scale of 0–3, with 0 marking normal condition and 3 representing extremely poor condition. Mice were selected for experiments when the sum of the first five category scores was greater than or equal to 6 or if the score of any individual category was equal to 3. All HD mice used experienced weight loss of 10–20% of their maximum weight. Mice were killed by inhalation of a saturating dose of isoflurane for at least 1 min, followed by cervical dislocation.

Electrical Recordings. *Flexor digitorum brevis* and *interosseous* muscle fibers were surgically removed, pinned to Sylgard-bottomed Petri dishes, and enzymatically dissociated at 35–36 °C under mild agitation for ~1 h using 1,000 U/mL of collagenase type IV (Worthington Biochemical). Collagenase was dissolved in the extracellular solution used for recording action potentials (below). Dissociation was completed using mild trituration in buffer with no collagenase. The fibers were allowed to recover at 21–23 °C for 1 h before being used for electrical measurements.

Fibers were visualized in an Olympus BX51WI microscope, and images were acquired with a CCD camera (ST-7XMEI-C1, Santa Barbara Instruments). Estimates of fiber surface area and volume were made assuming a cylindrical shape with ImageJ (National Institutes of Health) and SigmaPlot 11 (Systat Software). Electrical properties were measured under standard current and voltage clamp conditions at 21–23 °C using two aluminosilicate intracellular microelectrodes (part 30-0110, Harvard Apparatus), an Axoclamp 900A amplifier, a Digidata 1440a digitizer, and pCLAMP 10 data acquisition and analysis software (Molecular Devices). The voltage-sensing electrode was connected with an Axoclamp HSx1 headstage. The current-passing electrode was connected with an Axoclamp HSx10 headstage that was modified to have a 2-MΩ output resistor (HSx5). Both the current-passing and voltage-sensing electrodes were filled with the same solution (below). Data were acquired at 100 kHz. Current and voltage records were low-pass filtered with the internal Axoclamp 900A filters as follows: action potentials at 6 kHz and voltage clamp signals at 2 or 4 kHz. The voltage clamp command signal was low-pass filtered with an external Warner LFP-8 at 2 or 4 kHz. Filtering the voltage clamp records at 2 or 4 kHz produced no difference in measurements of peak current, conductance, or capacitance.

The internal (electrode) and extracellular solutions are listed below. The average electrode resistance was 13.5 ± 0.4 MΩ in current clamp experiments and 7.8 ± 0.3 MΩ in voltage clamp experiments. After impalement, 20 min was given for equilibration of the electrode solution with the sarcoplasm before data acquisition. EGTA was used in the internal solutions to prevent contractions.

Internal and Extracellular Buffers. Internal solution for action potentials and G_{Kir} (in mM) was as follows: 75 aspartate, 30 EGTA, 15 $Ca(OH)_2$, 5 $MgCl_2$, 5 ATP di-Na, 5 phosphocreatine di-Na, 5 glutathione, 20 Mops, and pH 7.2 with KOH (190 K^+).

Internal solution for G_{ClC-1} (in mM) was as follows: 17 aspartate, 30 HCl, 30 EGTA, 15 $CaCl_2$, 5 $MgCl_2$, 5 ATP di-Na, 5 phosphocreatine di-Na, 5 glutathione, 20 Mops, and pH 7.2 with CsOH.

Extracellular solution for action potentials (in mM) was as follows: 135 NaCl, 2.5 KCl, 5 $CaCl_2$, 2 $MgCl_2$, 5 glucose, 1 NaH_2PO_4, 10 Mops, and pH 7.2 with NaOH.

Extracellular G_{ClC-1} solution (in mM) was as follows: 140 HCl, 10 CsOH, 5 $CaCl_2$, 2 $MgCl_2$, 5 glucose, 1 NaH_2PO_4, 10 Mops, 0.0002 tetrodotoxin, 0.02 nifedipine, and pH 7.2 with tetraethylammonium hydroxide. 0.4 anthracene-9-carboxylic acid was added for G_{ClC-1} blocking solution.

Extracellular G_{Kir} solution (in mM) was as follows: 130 KCl, 12.5 NaCl, 5 $CaCl_2$, 2 $MgCl_2$, 5 glucose, 1 NaH_2PO_4, 10 Mops, 0.0002 tetrodotoxin, 0.02 nifedipine, 0.4 anthracene-9-carboxylic acid, and pH 7.2 with NaOH. 5 $BaCl_2$ was added for G_{Kir} blocking solution.

We recorded action potentials in fibers with a similar baseline membrane potential (between −80 and −90 mV) by applying a constant holding current of absolute magnitude <−5 nA (−3.3 ± 0.2 nA) for HD fibers and <−15 nA (−7.8 ± 0.9 nA) for WT fibers. Some current injection was necessary to compensate for damage caused by electrode impalement. All action potentials analyzed had peak amplitudes >110 mV.

mRNA Analysis. Total muscle RNA was isolated and 1 μg of RNA was reverse transcribed (46). To quantify total *Clcn1* and *Kcnj2* mRNA levels, real-time quantitative RT-PCR was performed with a BioRad DNA engine Opticon 2. *Clcn1* was quantified using primers that spanned either exons 10–14 or exons 16–19 as previously described (31). *Kcnj2* was quantified using a Taqman assay (Mm00434616.m1, Applied Biosystems). *Clcn1* and *Kcnj2* were normalized to β2-microglobulin (Taqman assay Mm00437762.m1, Applied Biosystems) and analyzed using the ΔΔCT method. For analysis of alternatively spliced gene products (inclusion of exon 7a) of *Clcn1*, PCR was performed as previously described (31), using primers that spanned the exon 7a site. PCR products were separated and stained with ethidium bromide. The amplicon containing exon 7a (420 bp) was quantified relative to the total including the normal adult *Clcn1* amplicon without exon 7a (341 bp).

Curve Fitting. Data analysis was accomplished with pCLAMP 10 and SigmaPlot 11. The action potential repolarizing phase was fitted with a double exponential,

$$f(x) = y_o + A_1 e^{-\frac{t}{\tau_1}} + A_2 e^{-\frac{t}{\tau_2}},$$

where y_o is the offset; A_1 and A_2 are amplitudes for components 1 and 2; and τ_1 and τ_2 are the decay constants of components of 1 and 2. Chloride channel relative open probability data were fitted with a Boltzmann curve (47),

$$P_o = \frac{1}{1 + e^{-\left(\frac{V_m - V_{0.5}}{k}\right)}},$$

where P_o is the relative open probability, V_m is the test potential, $V_{0.5}$ is the voltage at half-maximal activation, and k is the slope factor. Linear fits were used to determine conductance values.

Statistical Analysis. Means of two independent samples were compared using a two-tailed *t* test when the data were found normal by the Shapiro-Wilk test and had equal variances based on a folded *F* variance ratio test. For nonnormal and/or heteroscedastic samples we used the Mann-Whitney rank sum test. Null hypotheses in all statistical tests were rejected at $\alpha \leq 0.05$. Mean values are presented as ±SEM.

Chemicals. Chemicals were purchased from Fisher Scientific; exceptions include $CaCl_2$ and $MgCl_2$ (TekNova), CsOH and tetraethylammonium hydroxide (Alfa Aesar), ATP di-Na and nifedipine (Sigma-Aldrich), $BaCl_2$ (Matheson, Colman and Bell), tetrodotoxin (Abcam), and anthracene-9carboxylic acid (Tocris).

ACKNOWLEDGMENTS. We thank Dr. Sepehr Eskandari (California State Polytechnic University, Pomona) for discussions, editorial comments, and most notably for providing financial support to test the hypothesis of a new faculty member before external funds were awarded; Mrs. Cynthia Tessler for helping to devise and oversee animal care and Dr. David Moriarty for statistical advice (both from the California State Polytechnic University, Pomona); and Drs. Julio L. Vergara and Marino DiFranco for numerous technical and experimental discussions and Drs. Donald D. F. Loo and Thomas M. Vondriska for editorial comments (all from the University of California, Los Angeles David Geffen School of Medicine). This work was supported by a California State University Program for Education and Research in Biotechnology (CSUPERB) New Investigator S12 grant and was supported in part by National Institutes of Health/National Institute of General Medical Sciences Grant 1SC3GM096945 (to A.A.V.).

1. Bett JS, Bates GP, Hockly E (2006) Molecular pathogenesis and therapeutic targets in Huntington's disease. *Genetic Instabilities and Neurological Diseases*, eds Wells RD, Ashizawa T (Elsevier/Academic Press, Boston), 2nd Ed, pp 223–249.
2. Lo DC, Hughes RE (2010) *Neurobiology of Huntington's Disease: Applications to Drug Discovery* (CRC/Taylor & Francis Group, Boca Raton, FL) p 312.
3. Arenas J, et al. (1998) Complex I defect in muscle from patients with Huntington's disease. *Ann Neurol* 43(3):397–400.
4. Busse ME, Hughes G, Wiles CM, Rosser AE (2008) Use of hand-held dynamometry in the evaluation of lower limb muscle strength in people with Huntington's disease. *J Neurol* 255(10):1534–1540.
5. Lodi R, et al. (2000) Abnormal in vivo skeletal muscle energy metabolism in Huntington's disease and dentatorubropallidoluysian atrophy. *Ann Neurol* 48(1):72–76.
6. Ribchester RR, et al. (2004) Progressive abnormalities in skeletal muscle and neuromuscular junctions of transgenic mice expressing the Huntington's disease mutation. *Eur J Neurosci* 20(11):3092–3114.
7. Saft C, et al. (2005) Mitochondrial impairment in patients and asymptomatic mutation carriers of Huntington's disease. *Mov Disord* 20(6):674–679.
8. Sassone J, Colciago C, Cislaghi G, Silani V, Ciammola A (2009) Huntington's disease: The current state of research with peripheral tissues. *Exp Neurol* 219(2):385–397.
9. Sathasivam K, et al. (1999) Formation of polyglutamine inclusions in non-CNS tissue. *Hum Mol Genet* 8(5):813–822.
10. She P, et al. (2011) Molecular characterization of skeletal muscle atrophy in the R6/2 mouse model of Huntington's disease. *Am J Physiol Endocrinol Metab* 301(1): E49–E61.
11. Strand AD, et al. (2005) Gene expression in Huntington's disease skeletal muscle: A potential biomarker. *Hum Mol Genet* 14(13):1863–1876.
12. Turner C, Cooper JM, Schapira AH (2007) Clinical correlates of mitochondrial function in Huntington's disease muscle. *Mov Disord* 22(12):1715–1721.
13. Hodgkin AL, Horowicz P (1959) The influence of potassium and chloride ions on the membrane potential of single muscle fibres. *J Physiol* 148:127–160.
14. Adrian RH, Bryant SH (1974) On the repetitive discharge in myotonic muscle fibres. *J Physiol* 240(2):505–515.
15. Bryant SH, Morales-Aguilera A (1971) Chloride conductance in normal and myotonic muscle fibres and the action of monocarboxylic aromatic acids. *J Physiol* 219(2): 367–383.
16. Hutter OF, Noble D (1960) The chloride conductance of frog skeletal muscle. *J Physiol* 151:89–102.
17. Klocke R, Steinmeyer K, Jentsch TJ, Jockusch H (1994) Role of innervation, excitability, and myogenic factors in the expression of the muscular chloride channel ClC-1. A study on normal and myotonic muscle. *J Biol Chem* 269(44):27635–27639.
18. Pusch M, Jentsch TJ (1994) Molecular physiology of voltage-gated chloride channels. *Physiol Rev* 74(4):813–827.
19. Steinmeyer K, et al. (1991) Inactivation of muscle chloride channel by transposon insertion in myotonic mice. *Nature* 354(6351):304–308.
20. Steinmeyer K, Ortland C, Jentsch TJ (1991) Primary structure and functional expression of a developmentally regulated skeletal muscle chloride channel. *Nature* 354(6351): 301–304.
21. Mangiarini L, et al. (1996) Exon 1 of the HD gene with an expanded CAG repeat is sufficient to cause a progressive neurological phenotype in transgenic mice. *Cell* 87(3):493–506.
22. The Huntington's Disease Collaborative Research Group (1993) A novel gene containing a trinucleotide repeat that is expanded and unstable on Huntington's disease chromosomes. *Cell* 72(6):971–983.
23. Hickey MA, Gallant K, Gross GG, Levine MS, Chesselet MF (2005) Early behavioral deficits in R6/2 mice suitable for use in preclinical drug testing. *Neurobiol Dis* 20(1): 1–11.
24. Carter RJ, et al. (1999) Characterization of progressive motor deficits in mice transgenic for the human Huntington's disease mutation. *J Neurosci* 19(8):3248–3257.
25. Lione LA, et al. (1999) Selective discrimination learning impairments in mice expressing the human Huntington's disease mutation. *J Neurosci* 19(23):10428–10437.
26. Murphy KP, et al. (2000) Abnormal synaptic plasticity and impaired spatial cognition in mice transgenic for exon 1 of the human Huntington's disease mutation. *J Neurosci* 20(13):5115–5123.
27. Berg J, Jiang H, Thornton CA, Cannon SC (2004) Truncated ClC-1 mRNA in myotonic dystrophy exerts a dominant-negative effect on the Cl current. *Neurology* 63(12): 2371–2375.
28. Charlet-B N, et al. (2002) Loss of the muscle-specific chloride channel in type 1 myotonic dystrophy due to misregulated alternative splicing. *Mol Cell* 10(1):45–53.
29. Chen MF, Niggeweg R, Iaizzo PA, Lehmann-Horn F, Jockusch H (1997) Chloride conductance in mouse muscle is subject to post-transcriptional compensation of the functional Cl- channel 1 gene dosage. *J Physiol* 504(Pt 1):75–81.
30. Galka-Marciniak P, Urbanek MO, Krzyzosiak WJ (2012) Triplet repeats in transcripts: structural insights into RNA toxicity. *Biol Chem* 393(11):1299–1315.
31. Hao M, et al. (2008) Muscleblind-like 2 (Mbnl2) -deficient mice as a model for myotonic dystrophy. *Dev Dyn* 237(2):403–410.
32. Lueck JD, et al. (2007) Chloride channelopathy in myotonic dystrophy resulting from loss of posttranscriptional regulation for CLCN1. *Am J Physiol Cell Physiol* 292(4):C1291–C1297.
33. Mankodi A, et al. (2000) Myotonic dystrophy in transgenic mice expressing an expanded CUG repeat. *Science* 289(5485):1769–1773.
34. Mankodi A, et al. (2002) Expanded CUG repeats trigger aberrant splicing of ClC-1 chloride channel pre-mRNA and hyperexcitability of skeletal muscle in myotonic dystrophy. *Mol Cell* 10(1):35–44.
35. Mykowska A, Sobczak K, Wojciechowska M, Kozlowski P, Krzyzosiak WJ (2011) CAG repeats mimic CUG repeats in the misregulation of alternative splicing. *Nucleic Acids Res* 39(20):8938–8951.
36. Yuan Y, et al. (2007) Muscleblind-like 1 interacts with RNA hairpins in splicing target and pathogenic RNAs. *Nucleic Acids Res* 35(16):5474–5486.
37. DiFranco M, Herrera A, Vergara JL (2011) Chloride currents from the transverse tubular system in adult mammalian skeletal muscle fibers. *J Gen Physiol* 137(1):21–41.
38. Fahlke C (2001) Ion permeation and selectivity in ClC-type chloride channels. *Am J Physiol Renal Physiol* 280(5):F748–F757.
39. Fahlke C, Rüdel R (1995) Chloride currents across the membrane of mammalian skeletal muscle fibres. *J Physiol* 484(Pt 2):355–368.
40. Lueck JD, Rossi AE, Thornton CA, Campbell KP, Dirksen RT (2010) Sarcolemmal-restricted localization of functional ClC-1 channels in mouse skeletal muscle. *J Gen Physiol* 136(6):597–613.
41. Standen NB, Stanfield PR (1980) Rubidium block and rubidium permeability of the inward rectifier of frog skeletal muscle fibres. *J Physiol* 304:415–435.
42. Standen NB, Stanfield PR (1979) Potassium depletion and sodium block of potassium currents under hyperpolarization in frog sartorius muscle. *J Physiol* 294:497–520.
43. Ariano MA, et al. (2005) Striatal potassium channel dysfunction in Huntington's disease transgenic mice. *J Neurophysiol* 93(5):2565–2574.
44. Ashcroft FM, Heiny JA, Vergara J (1985) Inward rectification in the transverse tubular system of frog skeletal muscle studied with potentiometric dyes. *J Physiol* 359:269–291.
45. Dassau L, Conti LR, Radeke CM, Ptáček LJ, Vandenberg CA (2011) Kir2.6 regulates the surface expression of Kir2.x inward rectifier potassium channels. *J Biol Chem* 286(11): 9526–9541.
46. Talmadge RJ, Garcia ND, Roy RR, Edgerton VR (2004) Myosin heavy chain isoform mRNA and protein levels after long-term paralysis. *Biochem Biophys Res Commun* 325(1):296–301.
47. Pusch M, Steinmeyer K, Koch MC, Jentsch TJ (1995) Mutations in dominant human myotonia congenita drastically alter the voltage dependence of the ClC-1 chloride channel. *Neuron* 15(6):1455–1463.